Geomechanical Modeling for Thermal Spallation Drilling.

Stuart D.C. Walsh, Ilya Lomov, and Jeffery J. Roberts
Lawrence Livermore National Laboratory

Keywords: Thermal spallation drilling, Numerical modeling, Engineered Geothermal Systems

Abstract

Wells for Engineered Geothermal Systems (EGS) typically occur in conditions presenting significant challenges for conventional rotary and percussive drilling technologies: granitic rocks that reduce drilling speeds and cause substantial equipment wear. Thermal spallation drilling, in which rock is fragmented by high temperature rather than mechanical means, offers a potential solution to these problems. However, much of the knowledge surrounding this drilling technique is empirical - based on laboratory experiments that may or may not represent field conditions. There is a lack of understanding coupled with large uncertainties in the phenomenology of the process which could be resolved with computer modeling.

System-scale simulations of thermal spallation employ phenomenological models of rock damage due to the thermal gradient and erosion of spalls by the fluid. This allows rapid evaluation of mass and energy balances near the drill head and parametric studies of the relationship between drilling performance and the parameters of the jet. However, large-scale modeling is not suitable for resolving rock grains and inhomogeneities, and the damage model must account for the temperature gradient – not typically used as an input parameter in such material models. Thus, the parameters governing such phenomenological damage models require calibration by mesoscale simulations that fully resolve rock grains.

This paper outlines a new numerical modeling effort investigating the grain-scale processes governing thermal spallation drilling. Several factors affect spall production at the mesoscale, including grain size and size distribution, surface temperatures and material heterogeneity. To investigate the relative influence of these factors, we have conducted a series of simulations using GEODYN – a parallel Eulerian solid and fluid dynamics code. In this paper, we describe a two-dimensional model used to simulate the grain-scale processes and present preliminary results from this modeling effort.

1 Introduction

Drilling costs account for 30-60% of the total capital investment required for a geothermal or Enhanced Geothermal System (EGS) well [29] These costs are dominated by expenses resulting from slow drilling rates in granitic rocks and time-lost for equipment replacement [28]. New drilling technologies are required to lower this capital investment and to facilitate the development of relatively low emission renewable geothermal energy production on a competitive basis with other technologies. Thermal spallation - in which rock is fragmented by extreme heat - promises more rapid drilling of hard brittle rocks compared to conventional mechanical drilling techniques. Moreover, the drill suffers minimal wear as the bit head is not in contact with the rock [10, 21]. However, to date, the theory describing these drilling techniques is largely based on laboratory and near-surface experiments, which may not be representative of conditions at depth or properly account for variations in rock types. Consequently, there is a need for accurate numerical models of thermal spallation to help address uncertainties in this process.

This paper outlines some of the critical issues and needs of thermal spallation drilling (TSD) as a new drilling technology that can be addressed by computational modeling of the process. We describe a computationally rigorous modeling approach that incorporates key physics and micromechanics that will lead to improved understanding of the thermal spallation. Specifically, the model couples the grain-scale thermomechanics of spallation with system-scale

simulations of fluid dynamics and heat transfer to the rock face. Here, we focus primarily on the grain-scale model describing the micromechanical aspects of rock damage under sharp temperature gradients.

Thermal-spallation drilling was first employed in the 1940's to prepare blast holes for Taconite mines, and later used in granite quarrying and well drilling [6,24]. Early drilling methods utilized flame-jet spallation, where a high-temperature torch serves as the heat source. Since then, a variety of thermal spallation techniques have been implemented, primarily distinguished by the method used to deliver heat to the rock-face – examples include hydrothermal flame, laser, and microwave spallation [20, 21]. Nevertheless, the process by which spalls are produced is thought to be similar in each case; following a mechanism first proposed by Preston to describe brick spallation [22, 23]:

1. Heating the rock produces large temperatures, and associated compressive-stresses, which are confined close to the surface due to the rock's low thermal conductivity.
2. The compressive stresses generate fractures parallel to the rock surface from pre-existing flaws.
3. Upon reaching a critical ratio of surface-area to width, the heated fragments adjacent to the surface buckle and are ejected as spalls (Figure 1).

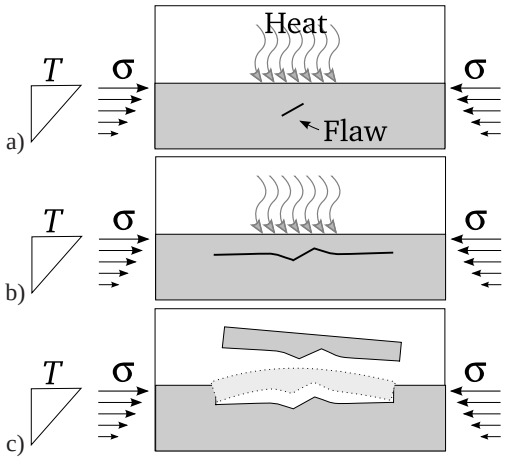

Figure 1: Simplified illustration of spall-production. a) Applied heat flux causes compressive stresses adjacent to the surface. b) Fractures grow parallel to the surface from incipient flaws in the rock. c) Upon reaching a critical ratio of surface-area to width, spalls buckle and are ejected from the surface.

Building on Preston's mechanism of spall production, Dey and Kranz [8, 9] employed plate-buckling theory to bound the heat flux required to generate spalls from a granite surface. Their analysis estimated spall rates by relating heat penetration depths to an assumed Weibull distribution of fracture-nucleation sites within the rock mass. Later, Rauenzahn and Tester [25] and Wilkinson and Tester [30], combined this approach with a fluid dynamics model to calculate thermal spallation drilling rates and drilling hole profiles for flame-jet spallation under steady state conditions. While the Tester group [25, 30] successfully matched simulated and experimental results, they noted that their approach was necessarily an empirical one. Stating that "[t]he good agreement between predictions and experiments could simply be the result of fortuitous cancellation of errors," they stressed the need for further studies investigating the multi-scale processes involved in TSD [30].

Detailed computer modeling can help address several of the uncertainties surrounding TSD. For example:

1. What rock compositions are drillable with TSD? There is experimental observation that some brittle rocks spall and some not, depending on composition.
2. Is thermal spallation driven by heterogeneities of the rock? If so, what incipient flaw distribution is sufficient for the process to work? How do grain size and grain size distribution affect TSD and drilling rates?
3. What combination of macroscopic (Poisson ratio, heat capacity and thermal conductivity) and microscopic (flaw distribution, tensile strength) characteristics favor thermal spallation?
4. How well do experimental results under lab conditions (relatively low confinement pressure and low ambient temperature) extrapolate to deep underground reservoir conditions? For example, some rocks can undergo high temperature brittle-ductile transitions that will make them harder to spall.

5. There is high mass content of rock debris in the bottom of the hole which can significantly alter heat transfer from the high temperature jet to the rock surface. Simulations can aid in quantifying these multiphase flow conditions.

6. Nozzle properties and jet shape and parameters could be optimized for a specific rock type for optimal drilling speed and energy efficiency.

In this paper, we describe a new numerical modeling effort to investigate the processes involved in TSD. These include interconnected phenomena on several length and time scales: from system-scale fluid dynamics and heat transfer to the rock face to the grain-scale thermomechanics of spallation. Here, we focus primarily on the grain-scale model describing the micromechanical aspects of rock damage under a sharp temperature gradient. In Section 2, we describe the grain-scale model; outlining the material parameters employed in the simulation and the process by which the granite microstructure is generated. Preliminary results from two-dimensional simulations examining the relative effects of temperature, surface conditions, grain size and grain-size distribution are given in Section 3. Conclusions and future work are discussed in Section 4.

2 Numerical model

The simulations presented in this paper are conducted using GEODYN – a parallel Eulerian compressible solid and fluid dynamics code with adaptive mesh refinement (AMR) capabilities [1, 17]. Among its many features are a high-order material interface reconstruction algorithm [14] and advanced constitutive models that incorporate salient features of the dynamic response of geologic media [26]. GEODYN is able to simulate materials under extremely large deformations, resolve details of wave propagation within grains with high accuracy, and uses a continuum damage mechanics approach to represent fracture. Consequently, the simulations are able to capture the effects of grain-scale heterogeneity both in terms of the material and geometric properties of the grains, and can reproduce fracture both along grain boundaries and within grains themselves.

The Eulerian framework of adaptive mesh refinement [3] is a relatively mature technique for dynamically applying high numerical resolution to those parts of a problem domain that require it, while solving less sensitive regions on less expensive, coarser computational grids. Adaptive mesh refinement can help to simulate the entire process region (or a significant portion thereof) while allowing focus on greater details in interesting locations. In combination, Eulerian Godunov methods with AMR have been proven to produce highly accurate and efficient solutions to shock capturing problems. The method used here is based on some modifications of the single-phase high-order Godunov method. This method is not as straightforward as Lagrangian FEM, so it will be briefly summarized below. For solid mechanics, the governing equations consist of the laws of conservation of mass, momentum and energy, an equation for distortional elastic deformation, and a number of equations in a form of

$$\frac{\partial}{\partial t}\left(\rho F_i\right) + \nabla \cdot \left(\rho \mathbf{v} F_i\right) = \rho \Phi_i, \tag{1}$$

which represent specific rheological equations $\dot{F}_i = \Phi_i$ (a superposed dot denotes material time differentiation) for history dependent parameters F_i (like porosity, plastic strain, etc.). The viscoplasticity is modelled with a measure of elastic deformation as a symmetric, invertible, positive definite tensor $\mathbf{B}_e$, which is determined by integrating the evolution equation

$$\dot{\mathbf{B}}'_e = \mathbf{L} \cdot \mathbf{B}'_e + \mathbf{B}'_e \cdot \mathbf{L}^\top - 2/3\mathbf{L} : \mathbf{I} - \mathbf{A}_d \,, \tag{2}$$

where $\mathbf{L}$ denotes the velocity gradient [27]. It is possible to define a unimodular tensor which is a pure measure of elastic distortional deformation $\mathbf{B}'_e$. In traditional von Mises materials shear stresses depend purely on $\mathbf{B}'_e$. The inelastic deviatoric deformation tensor $\mathbf{A}_d$ can be written as:

$$\mathbf{A}_d = \Gamma_d \left(\mathbf{B}'_e - \left(\frac{3}{\mathbf{B}'_e : \mathbf{I}} \right) \mathbf{I} \right) \,, \tag{3}$$

where the scalar rate functions Γ_d require constitutive equations. The rate-dependent formulation (3) can be easily converted to a rate-independent von Mises functional form.

The numerical scheme for a single fluid cell is based on the approach of [19], with some modifications to take into account the full stress tensor associated with solids. The multidimensional equations are solved by using an operator splitting technique, in which the one-dimensional equations for each direction are solved:

$$U_{i,\alpha}^{n+2} = S_H\left(S_{0,0,1}\left(S_{0,1,0}\left(S_{1,0,0}\left(S_H\left(S_{1,0,0}\left(S_{0,1,0}\left(S_{0,0,1}\left(U_{i,\alpha}^{n}\right)\right)\right)\right)\right)\right)\right)\right), \tag{4}$$

where the spatially split operators

$$S_{i_\beta,j_\beta,k_\beta}\left(U_{1,\ldots,l,\alpha}^{n+m/3}\right) \tag{5}$$

are applied in a Strang-splitting order to keep second-order accuracy, while the source term

$$S_H\left(U_{1,\ldots,l,\alpha}^{n,H}\right) = U_{1,\ldots,l,\alpha}^{n,H} + \Delta t V_\alpha H_\alpha\left(U_{1,\ldots,l,\alpha}^{n,H}\right) \tag{6}$$

is always applied at the end of the timestep. Each directional operator is the update of the cell from time step n to time step n+1 with fluxes computed at the cell's edges. Edge fluxes are calculated based on upwind characteristic tracing following [19] and to Riemann solver in an acoustic approximation. The estimate for the velocity gradient L in (6) is calculated in the Riemann solver step.

The biggest challenge in the Eulerian and multimaterial ALE methods is the treatment of mixed cells that contain several materials. The algorithm described here treats the propagation of surfaces in space in terms of an equivalent evolution of volume fractions defined by the equation:

$$\frac{\partial f_\alpha}{\partial t} + \nabla\cdot(f_\alpha \mathbf{v}) = \frac{f_\alpha}{K_\alpha} K \nabla\cdot\mathbf{v}, \tag{7}$$

where f_α and K_α are the volume fraction and the bulk modulus of each material α. The approach to modelling multimaterial cells is similar to that in [19]. Specifically, material properties have multiple values in a cell, but the velocity and stress are single-valued. In order to use the single-fluid solver, it is necessary to define an effective single phase for the mixed cells and to update material volume fractions based on self-consistent cell thermodynamics:

$$\begin{aligned} 1/K &= \sum f_\alpha/K_\alpha \qquad & T_{ii} &= 1/K \sum f_\alpha T_{ii\alpha}/K_\alpha \\ 1/G &= \sum f_\alpha/G_\alpha \qquad & T_{ij,i\neq j} &= 1/G \sum f_\alpha T_{ij\alpha}/G_\alpha \end{aligned} \tag{8}$$

where $G_\alpha, T_{ij\alpha}$ are the shear modulus and the stress tensor of material α. Distribution of the velocity gradient amongst each material in the cell required to integrate (2) for each material is done in a similar way:

$$\mathbf{L}_\alpha = \mathbf{L} G/G_\alpha\,. \tag{9}$$

In order to advect volume fractions, we use a high order interface reconstruction (interface tracking), which preserves linear interfaces during translation. Constraint on volume fractions is satisfied assuming fast equilibration of partial pressures in the cell. The pressure relaxation algorithm consists of iterative adjustments of volume fractions. First, average pressure is calculated:

$$p = \sum_\alpha \frac{f^\alpha p^\alpha}{K^\alpha} \Bigg/ \sum_\alpha \frac{f^\alpha}{K^\alpha}\ . \tag{10}$$

Next, the change of volume fraction for current iteration step is calculated:

$$\delta f_\alpha = \beta_\alpha f_\alpha (p^\alpha - p)\,./K^\alpha \tag{11}$$

The limiter β_a in (11) is chosen from numerical and physical considerations, i.e. all volume fractions should fall in the zero to one range, change of material density should be limited, etc.

Granite microstructures comprising three minerals – quartz, plagioclase, and potassium feldspar (or K-spar) – are considered in this paper. The mechanical properties assigned to each mineral are taken from Bass [2] and Mavko

Mineral	Density	Bulk modulus	Poisson ratio	Heat Capacity	Thermal conductivity
Quartz	2.65 g/cm^3	37.0 GPa	0.08	0.93 J/g.K	7.7 W/m.K
Plagioclase	2.56 g/cm^3	50.8 GPa	0.26	0.93 J/g.K	1.5 W/m.K
K-spar	2.63 g/cm^3	53.7 GPa	0.28	0.93 J/g.K	1.5 W/m.K

Table 1: Material properties by mineral type.

et al. [18] and are summarized in Table 1. In addition, the inter-grain contacts are represented by a separate, weaker material with compressive and tensile strengths based on grain-contact properties given in Lan et al [16]. The minerals' constitutive behavior is modeled as elastic-perfectly plastic, with a pressure dependent Von-Mises yield criteria:

$$Y = \sqrt{k(p - p_c)}\,, \tag{12}$$

where k is a material parameter and $p_c = (1 - D)p_{c_0}$ is a damage-dependent pressure cut-off. The parameters, k and p_{c_0} are determined from the minerals' tensile and compressive strengths, while damage, D, is calculated from the plastic strain according to a Johnson-Cook damage rule [15]:

$$D = \int \frac{|d\epsilon_p|}{\epsilon_f}\,, \tag{13}$$

where ϵ_p is the plastic strain, and ϵ_f the strain to failure.

Heat capacities and relative thermal conductivities for each mineral are based on values reported in Findikakis [12] and Clauser & Huenges [7]. As the rate at which heat is transmitted into the rock ($O(m/h)$) is significantly slower than the speed of fracture propagation ($O(km/s)$), we artificially increase the thermal conductivities by a factor of $10,000$. This maintains a quasi-static temperature profile over fracture timescales while reducing simulation times to manageable levels. In this paper, we consider thermal spallation due to conduction from a high temperature fluid adjacent to the rock surface (*e.g.* flame-jet or hydrothermal spallation), rather than radiative transfer (*e.g.* laser spallation). To avoid thermal shock in the simulations, the fluid adjacent to the rock is gradually heated from the initial rock temperature to the target surface temperature, and held at a constant temperature thereafter.

Geometric, as well as material, heterogeneties are also important in determining the behavior of aggregate materials. In particular, several studies have stressed the role that grain size and grain-size distribution play in the strength of crystalline rocks [4,11,13,16,31]. Here, the rock microstructure is created with an iterative approach that fits Voronoi-cell volumes to a target grain-size distribution. Although, two-dimensional simulations are presented here, the method is equally applicable in three dimensions. Voronoi cells are initially generated from a set of random points, and each cell assigned a target volume from a predetermined grain-size distribution. The Voronoi-cell volumes are then relaxed towards the target distribution over a series of iterations, in which the cell centers are updated according to:

$$\mathbf{X}_{new} = \mathbf{X}_{old} + \left[\frac{\partial \mathbf{V}}{\partial \mathbf{X}}\right]^{\dagger} (\mathbf{V}_{target} - \mathbf{V})\,, \tag{14}$$

where $\mathbf{X}$ is a vector of coordinates for the cell-centers; $\mathbf{V}$ and $\mathbf{V}_{target}$ are vectors of Voronoi-cell volumes and target volumes respectively; and $\mathrm{A}^{\dagger}$ indicates the pseudo-inverse of the matrix A. The iterative improvement is repeated until the average error in cell volumes is below a predetermined tolerance (typically less than 1% error in cell volumes).

3 Results

Images from a typical simulation illustrating fracture initiation and propagation are shown in Figure 2. Fractures commence at the weaker inter-grain boundaries, then propagate both along grain boundaries and within the grains themselves. This is consistent with experimental observations that spalls tend to form with maximum lengths several

grain-diameters in extent but with thicknesses less than an average grain diameter thick [24]. The direction of fracture propagation is largely aligned with the local compressive stress.

Surface conditions play a significant role in the onset and manner of spallation. In particular, artificially flat interfaces are less likely to fracture than rough surfaces. Asperities on the rock surface serve as focal points for spall initiation, as protruding crystals heat more rapidly than their neighbors. Conversely, simulations with a flat fluid-rock interface withstand substantially higher heat fluxes before spalling and the spalling mechanism also differs. In these cases, damage occurs predominantly along inter-grain boundaries and significantly larger spalls are generated (Figure 3) – suggesting that analyses employing classical beam and plate buckling theory in an semi-infinite half-space may over-estimate the compressive stress required for spall production. Higher surface temperatures cause earlier onset of spalling, and the formation of smaller fragments. This is illustrated in Figure 4, which compares damage versus time for different surface temperature increments. These results supports predictions by the Tester group that spalling rates should increase with temperature due to the greater likelihood of initiating new fracture nucleation sites [24].

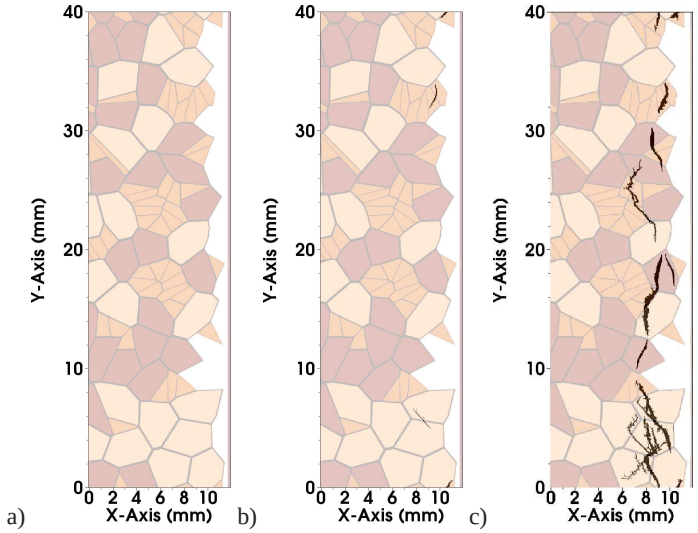

Figure 2: Fracture initiation and propagation in a typical simulation. a) Grain microstructure: beige colored grains are quartz; orange grains are k-spar; brown grains are plagioclase. The rock is heated by fluid in the voids on the right of the image. b) Fractures (in black) initiate at inter-grain boundaries, c) but then tend to propagate in the principal compressive stress direction.

Perhaps surprisingly, assemblies of smaller grains spall less readily than those with larger grains. This may be because the temperature distribution is more uniform in small-grain assemblies (Figure 5). As a result of differences in thermal conductivity, assemblies with larger quartz grains transmit heat more rapidly into the rock body, and experience less uniform stress fields. However, the reduced tendency to spall may also be linked to the surface roughness, which is decreased in assemblies with smaller grains. Assemblies with heterogeneous grain size distributions with large quartz grains also experience greater variation in temperature distribution (Figure 5c) and, for similar reasons, tend to spall more readily than those with uniform grains.

Increasing confining pressure results in the production of larger spalls and reduces

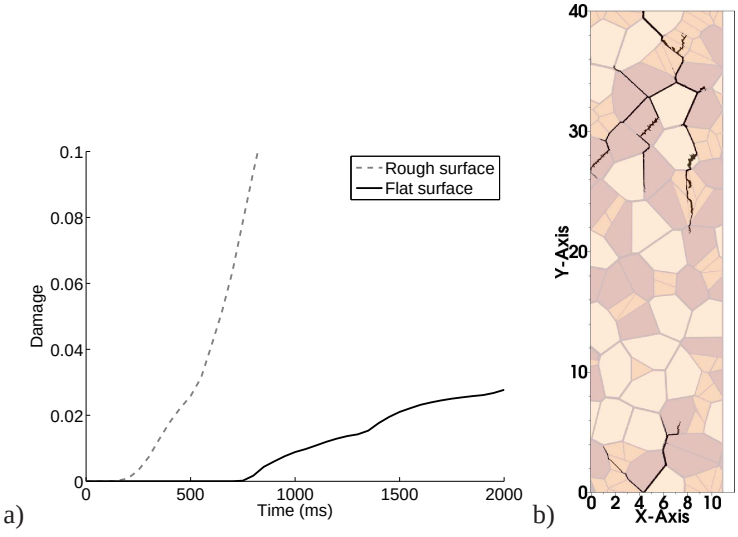

Figure 3: a) Damage as a function of time for simulations with flat and rough surfaces. b) Fractures in flat surface simulation.

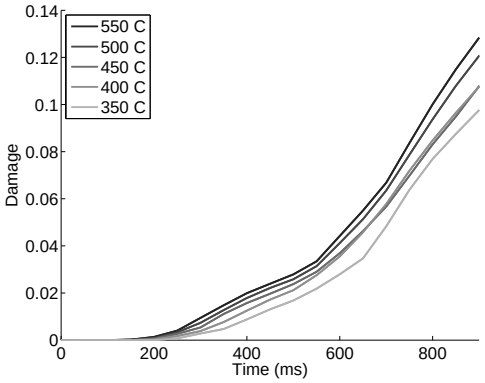

Figure 4: Damage as a function of time for different surface temperatures.

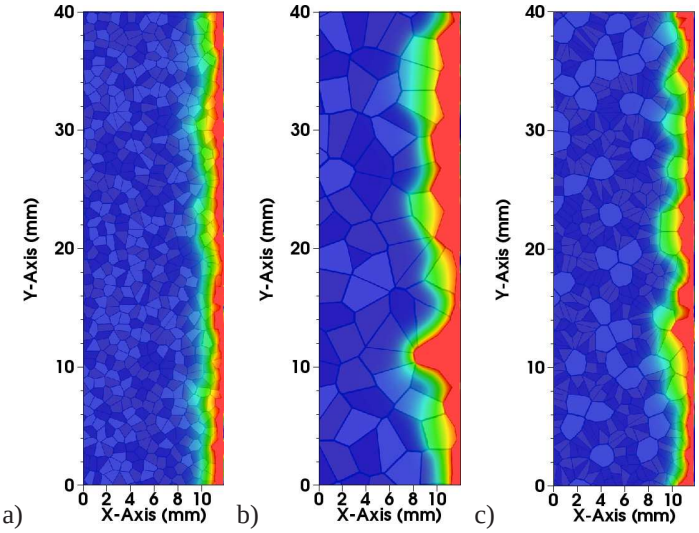

Figure 5: Temperature distribution in simulations with varying grain sizes: a) 1 mm mean grain diameter b) 3 mm mean grain diameter c) 2 mm quartz grain diameter, and 1 mm mean diameter for other grains.

damage (Figure 6). At first glance, this prediction appears in conflict with results from field tests of flame-jet spallation, which report increased drilling rates with depth [5]. However, increased drilling rates in the field have been attributed to chemical and macrostructural differences – less oxidized and more competent rocks at depth spall more readily than damaged and weathered rock encountered near the surface [5, 6]. Alternatively, this result might also be explained by differences between simulated and operating conditions. The present two-dimensional model assumes equilibrium between the formation and fluid pressure to avoid damage from inconsistent initial conditions. However, this is not true of flame-jet spallation drilling systems at depth, as there is no drilling fluid to balance lithostatic stresses. We are currently developing a three dimensional version of the model with the goal of examining the role of hoop-stresses on spall production, which will address these issues.

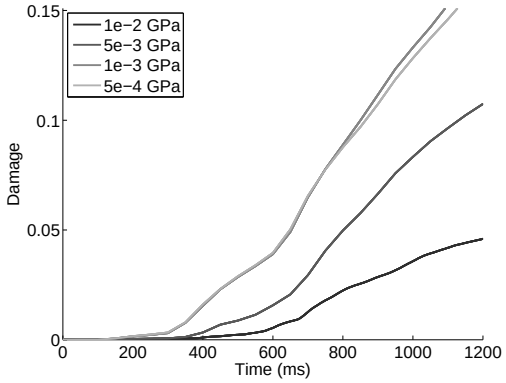

Figure 6: Damage as a function of time for different confining pressures.

4 Conclusion and future work

This paper describes a model for simulating thermal spallation at the grain scale, and presents results from two dimensional simulations that examine the qualitative effects of grain-size, grain-size distribution, surface temperature increase and surface roughness on spall creation. These preliminary results demonstrate the important role that heterogeneous material and grain properties play in determining the material response – factors that would be difficult or impossible to investigate with empirical continuum scale models.

These simulations represent the initial stages in a larger modeling effort to develop an integrated simulation environment coupling thermal spall and particle-laden flows. While the response of solids and structures are more easily treated by Lagrangian methods, the fluid and particulate flow are best handled in an Eulerian framework. Hence, we have chosen to use an Eulerian approach for both rock and fluid mechanics, with the added benefit of avoiding a labor-intensive mesh generation step. Debris accumulation can be a critical process which controls heat transfer to the rock face. Future mesoscale modeling of the removal of spalled rock debris by high-temperature, high-speed fluid flow will help to determine characteristics of the multiphase flow in the borehole, and incorporate our understanding of damage and multiphase flow on the mesoscale level. The developed integrated simulation tool will provide a predictive capability for modeling thermal spallation drilling useful for process optimization in practical applications.

5 Acknowledgments

This work was performed under the auspices of the U.S. Department of Energy by Lawrence Livermore National Laboratory under Contract DE-AC52-07NA27344.

References

[1] ANTOUN, T. H., LOMOV, I. N., AND GLENN, L. A. Development and application of a strength and damage model for rock under dynamic loading. In *Proceedings of the 38th U.S. Rock Mechanics Symposium, Rock Mechanics in the National Interest* (2001), D. Elsworth, J. Tinucci, and K. Heasley, Eds., A. A. Balkema Publishers, p. 369374.

[2] BASS, J. D. Elasticity of minerals, glasses, and melts. In *Mineral Physics and CrystallographyHandbook of Physical Constants, AGU Reference Shelf, Vol 2*, T. J. Ahrens, Ed. American Geophysical Union, 1995, pp. 45–63.

[3] BERGER, M. J., AND COLELLA, P. Local adaptive mesh refinement for shock hydrodynamics. *Journal of Computational Physics 82*, 1 (May 1989), 64–84.

[4] BLAIR, S., AND COOK, N. Analysis of compressive fracture in rock using statistical techniques: Part ii. effect of microscale heterogeneity on macroscopic deformation. *International Journal of Rock Mechanics and Mining Sciences 35*, 7 (1998), 849 – 861.

[5] BROWNING, J. A., HORTON, W. B., AND HARTMAN, H. L. Recent advances in flame jet working of minerals. In *7th Symposium on Rock Mechanics*. Pennsylvania State University, 1965.

[6] CALAMAN, J. J., AND ROLSETH, H. C. Technical advances expand use of jet-piercing process in taconite industry. In *International Symposium on Mining Research*. U.S. Bureau of Mines, 1961, pp. 473–498.

[7] CLAUSER, C., AND HUENGES, E. Thermal conductivity of rocks and minerals. In *Rock Physics and Phase Relations Handbook of Physical Constants, AGU Reference Shelf, Vol 3*, T. J. Ahrens, Ed. American Geophysical Union, 1995, pp. 105–126.

[8] DEY, T. N., AND KRANZ, R. L. Methods for increasing drilling performance of the thermal spallation drilling system. *GRC Transactions 9* (1985), 103–106.

[9] DEY, T. N., AND KRANZ, R. L. Flake mechanics, borehole breakouts and thermal spallation. In *Proceedings of the 28th US Symposium on Rock Mechanics* (1987), I. Farmer, J. Daemen, C. Desai, C.E.Glass, and S. Neuman, Eds.

[10] DREESEN, D., AND BRETZ, R. Coiled-tubing-deployed hard rock thermal spallation cavity maker: Phase 1 final report. *DOE Report (FWP-02FE15)* (2005).

[11] EBERHARDT, E., STIMPSON, B., AND STEAD, D. Effects of grain size on the initiation and propagation thresholds of stress-induced brittle fractures. *Rock Mechanics and Rock Engineering 32* (1999), 81–99. 10.1007/s006030050026.

[12] FINDIKAKIS, A. Heat capacity analysis report. *Bechtel SAIC Company* (2004), DOE Technical Report (ANL–NBS–GS–000013, REV 01).

[13] FREDRICH, J. T., EVANS, B., AND WONG, T.-F. Effect of grain size on brittle and semibrittle strength: Implications for micromechanical modelling of failure in compression. *Journal of Geophysical Research 95*, B7 (1990), 10,907–10,920.

[14] HERTEL, E. S. J., AND BELL, R. L. *An improved material interface reconstruction algorithm for Eulerian codes*. Sandia Nat Lab, 1992.

[15] JOHNSON, G., AND COOK, W. Fracture characteristics of three metals subjected to various strains, strain rates, temperatures and pressures. *Engineering Fracture Mechanics 21*, 1 (1985), 31–48.

[16] LAN, H., MARTIN, C. D., AND HU, B. Effect of heterogeneity of brittle rock on micromechanical extensile behavior during compression loading. *J. Geophys. Res. 115* (2010).

[17] LOMOV, I., AND RUBIN, M. Numerical simulation of damage using an elastic-viscoplastic model with directional tensile failure. *Journal De Physique IV 110* (2003), 281286.

[18] MAVKO, G., MUKERJI, T., AND DVORKIN, J. *The Rock Physics Handbook. Tools for Seismic Analysis of Porous Media*. Cambridge University Press, 2003.

[19] MILLER, G. H., AND PUCKETT, E. G. A high-order godunov method for multiple condensed phases. *Journal of Computational Physics 128*, 1 (Oct 1 1996), 134–164.

[20] PIERCE, K., LIVESAY, B., AND FINGER, J. *Advanced Drilling Systems Study*. Sandia National Laboratories, 1996.

[21] POTTER, R. M., POTTER, J. M., AND WIDEMAN, T. W. Laboratory study and field demonstration of hydrothermal spallation drilling. *GRC Transactions 34* (2010), 249–252.

[22] PRESTON, F. W. The spalling of bricks. *Journal of the American Ceramic Society 9*, 10 (1926), 654–658.

[23] PRESTON, F. W., AND WHITE, H. E. Observations on spalling. *Journal of the American Ceramic Society 17*, 1-12 (1934), 137–144.

[24] RAUENZAHN, R., AND TESTER, J. Rock failure mechanisms of flame-jet thermal spallation drilling–theory and experimental testing. *International Journal of Rock Mechanics and Mining Sciences & Geomechanics Abstracts 26*, 5 (1989), 381 – 399.

[25] RAUENZAHN, R. M., AND TESTER, J. W. Numerical simulation and field testing of flame-jet thermal spallation drilling–1. model development. *International Journal of Heat and Mass Transfer 34*, 3 (1991), 795 – 808.

[26] RUBIN, M. B., AND LOMOV, I. A thermodynamically consistent large deformation elastic-viscoplastic model with directional tensile failure. *International Journal of Solids and Structures 40*, 17 (2003), 4299 – 4318.

[27] RUBIN, M. B., VOROBIEV, O. Y., AND GLENN, L. A. Mechanical and numerical modeling of a porous elastic-viscoplastic material with tensile failure. *International Journal of Solids and Structures 37*, 13 (Mar 2000), 1841–1871.

[28] TESTER, J., HERZOG, H., CHEN, Z., POTTER, R., AND FRANK, M. Prospects for universal geothermal energy from heat mining. *Science & Global Security 5* (1994), 99121.

[29] TESTER, J. W., ANDERSON, B., BATCHELOR, A., BLACKWELL, D., DIPIPPO, R., DRAKE, E., GARNISH, J., LIVESAY, B., MOORE, M., NICHOLS, K., PETTY, S., TOKSOZ, N., VEATCH, R., AUGUSTINE, C., BARIA, R., MURPHY, E., NEGRARU, P., AND RICHARDS, M. *The Future of Geothermal Energy: Impact of Enhanced Geothermal Systems (EGS) on the United States in the 21st Century*. Massachusetts Institute of Technology, 2006.

[30] WILKINSON, M. A., AND TESTER, J. W. Computational modeling of the gas-phase transport phenomena during flame-jet thermal spallation drilling. *International Journal of Heat and Mass Transfer 36*, 14 (1993), 3459 – 3475.

[31] WONG, R. H., CHAU, K., AND WANG, P. Microcracking and grain size effect in Yuen Long marbles. *International Journal of Rock Mechanics and Mining Sciences & Geomechanics Abstracts 33*, 5 (1996), 479 – 485.